Rare Metal Materials and Engineering
Volume 47, Issue 8, August 2018
Online English edition of the Chinese language journal

Available online at www.sciencedirect.com
ScienceDirect

Cite this article as: Rare Metal Materials and Engineering, 2018, 47(8): 2305-2311.

ARTICLE

Microstructure and Properties of Laser Additive Manufactured Fe-Cr-Ni-B Steel by Divided-area Process

Zhao Yuhui, Wang Zhiguo, Zhao Jibin, Shi Fan

Shenyang Institute of Automation, Chinese Academy of Sciences, Shenyang 110016, China

Abstract: This paper presented a fundamental investigation on the formation mechanism and compatibility of microstructure/mechanical property of Fe-Cr-Ni-B steel samples, which were built by the divided-area forming and integral connection methods. Results indicate that the stress at the edge of the specimen produced in additive manufacturing is reduced by the divided-area forming and integral connection method. According to the microstructure analysis using stereology microscopy/optical microscopy/scanning electron microscope/X-ray diffractometer/Schaeffler diagram, the macrostructure is distributed in strip band geometry and the microstructures consist of dendrites with the intermetallic phases containing austenite phase, boride/matrix eutectic phase. Additionally, the macrostructure strips near the bonding line bend to the building direction and are discontinuous because of the unique forming method. However, the microstructures and composition of the samples are homogeneous. Due to the existence of boride and the finer microstructures, mechanical properties analysis shows that the alloy has high hardness, high ultimate strength and bad deformability. The hardness distribution is homogeneous apart from some positions of the re-melting zone and the heat-affected zone near the bonding line, which have a relatively lower hardness because of differences in microstructure.

Key words: additive manufacturing; divided-area forming process; microstructure; property; steel

Additive manufacturing (AM) technology is widely used for investigations and applications in aviation and space, to make structural components with titanium alloy and super-alloy[1-3]. Iron-based alloy, which has important applications in the field of defense and civil industry, has draw researchers from the additive manufacturing field[4-7]. Recently, additive manufacturing technology is flourishing, but the limitations of material types and application areas restrict its application. Among all kinds of AM technologies, laser engineered net shaping (LENS) has some advantages in making large structure parts. However, the deformation and cracking always happen during LENS process, and these problems could be controlled by optimization of internal stress field. According to the research of Ibiye Aseibichin Roberts [8], the stress between the first cladding layer and substance was the largest one among all the layers. Due to this phenomenon, the samples made by LENS may crack with the building substance, and the cracking behavior mostly begins in the border position of the samples. Based on previous research, the border position's stress of large structure parts could be reduced by the divided-area forming and integral connection method, which means dividing the samples into many smaller parts, and forming the small parts individually by LENS, and connecting them to a whole part by LENS. Fig.1 is the schematic of different forming methods. At the same time, by the divided-area forming method additive manufacturing device could reduce the requirement of effective working track, and increase building efficiency.

A kind of Fe-Cr-Ni-B steel was selected in the present paper to study the possibility of making large molds by the divided-area forming and integral connection method, and the element boron can increase the hardness of building part. Many researchers have studied the microstructure and properties of steel by LENS integral forming. Mingming Ma et al. [9] reported that the fabrication of precision large-scale metal parts can be achieved under open-loop control by DLF

Received date: August 25, 2017
Foundation item: National Key Research and Development Program of China (2016YFB1100502)
Corresponding author: Wang Zhiguo, Master, Research Assistant, Equipment Manufacturing Technology Research Laboratory, Shenyang Institute of Automation, Chinese Academy of Sciences, Shenyang 110016, P. R. China, Tel: 0086-24-83601225, E-mail: wangzhiguo@sia.cn

technology. J. A. Cabral Miramontes[10] proposed that the addition of boron lead to formation of α-Fe and M_2B eutectic phase, and the appearance of M_2B phase increased the hardness of samples. Kaibin Li et al.[11] proposed that the micro-structure of multiple-layer laser cladding of 308L stainless steel consisted of a large number of columnar dendrites, which were made up of austenite and a small amount of δ ferrite phase. By using the CSC-MIG to make Fe-Cr-B based alloy, A. A. Sorour et al. [12] presented that the deposited microstructure consists of matrix phase and hyper-eutectic phase. P. Krakhmalev et al.[13] reported microstructure evolution in AISI 420 martensitic stainless steel made by SLM, and austenite reversion took place during the situ heat treatment. Hussam El Cheikh[14] proposed that the 316L steel samples build by DLF show a homogeneous microhardness in each layer apart from a higher microhardness in the first layer. H. Khalid Rafi et al.[15] provided that tensile failure of PH1 steel samples is mainly cleavage fracture. This paper discussed the structure and mechanical property of samples built by divided-area process.

1 Experiment

In this work a self-built coaxial nozzle was associated with a 6-DOF multi-joint Staubli robot and a 2000 W fiber laser with the nozzle diameter of 3 mm. The laser type was "YLS-2000" and the wave length was 1070~1080 μm. Spherical gas-atomized steel based powders supplied by Höganäs Belgium SA Ltd. were used, with particles size between 53 and 150 μm. The composition of the powder is listed in Table 1. A self-designed powder delivery system was used for injecting powder to the molten pool under the carrying of Ar gas. A stainless steel plate was used as the building platform which was fixed in the cooling systems.

The laser power of 1400 W, 6 mm/s scanning speed and 40% overlapping rate were used as manufacturing process parameters. The average layer thickness was near 0.45 mm. The scanning method of the divided-area forming and integral connection method is illustrated in Fig.2a. As show in Fig. 2a, the both sides zones of the sample were firstly formed, and then the middle zone was formed to connect the two former zones. In order to connect the former zones densely, the surface of the side zone inclined to the building direction. The bonding line (position 1 in Fig. 2a) represented the bonding

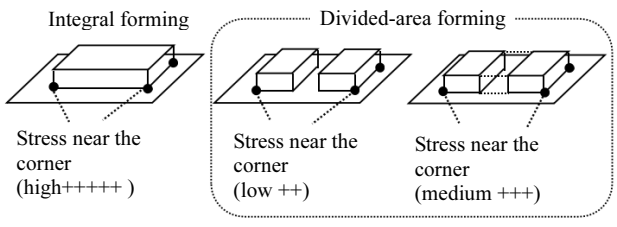

Fig.1 Schematic of the different forming method

Table 1 Chemical composition of Fe-Cr-Ni steel powder (wt%)

C	P	S	Mo	Ni	Mn	Cr	Si	B	Fe
0.13	0.01	0.01	1.4	4.4	0.6	15	1.3	0.8	Bal.

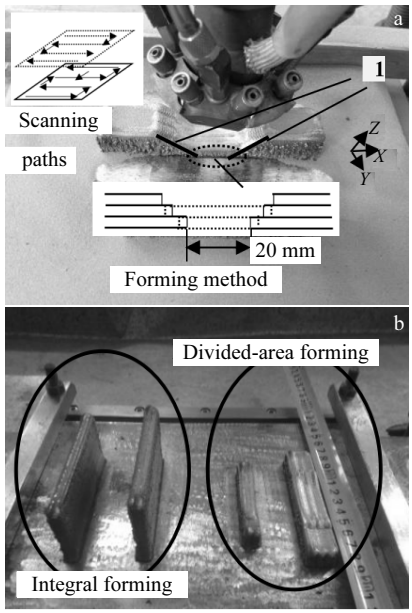

Fig.2 Process approach by divided-area forming: (a) forming principle and (b) processed parts

plane between middle and side zone of samples bent at ±45° with the building direction. Laser moved by zigzag scanning paths during the building process, while the adjacent layer scanning paths were reverse. In this paper, two block samples were built by the divided-area forming and integral connection method, with the size of 16 mm×70 mm×15 mm and 20 mm×100 mm×15 mm. The block samples were used for discussing the microstructure and hardness evolution. Two thin-wall samples were built by LENS with the same parameters for discussing the tensile property of samples at room temperature. The samples were with the same size of 8 mm×70 mm×60 mm, as shown in Fig. 2b.

Specimens were cut from the building platform, and then mounted, polished and etched with etchant (with volume ration of $HCl:HNO_3$=3:1). The etching time was 10 s. The microstructure of those specimens was observed by stereology microscopy (Stemi 2000), and optical microscopy (Axiovert 200 MAT). The element analysis was done by the energy dispersive spectrometry during scanning electron microscope (SEM) analysis. The phase constitutions of the specimens were identified by X-ray diffractometer (D/Max-2500PC).

The hardness was measured by Rockwell hardness tester and Vickers (AMH43). The Vickers microhardness was measured with an indentation load of 200 g for 15 s. The room temperature tensile testing was done with INSTRON 5582. The testing samples size is shown in Fig.3, and the testing samples were cut from thin-wall samples along the scanning direction.

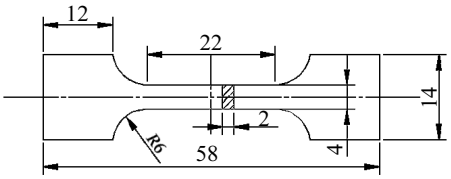

Fig.3 Tensile sample size

2 Results and Discussion

2.1 Microstructure

Fig.4 demonstrates the XZ cross-section microstructures of samples made by the divided-area forming. The positions of the microstructures observed in divided-area forming zone were away from the bonding line (Fig.2). The deposition microstructures were composed of dendrites with their growth orientation nearly parallel to the building direction. The microstructures between the adjacent layers were equiaxed grain zone. The growth type and direction of microstructure depended on the moving direction of molten pool, solidification temperature gradient (G) and crystal growth rate (R). Because of the rapid moving of molten pool during additive manufacturing, the heat transfer direction was nearly perpendicular to the molten pool's moving direction, and the unidirectional of heat transfer lead to epitaxial growth of solidification microstructures. According to microstructure demonstrated in Fig.4 the average thickness of one layer was about 0.4~0.5 mm, which is consistent with the building parameters. According to the observation of OM, on most positions of the samples made by divided-area forming, the microstructures were made up of the epitaxial growth dendrites (as shown at A zone in Fig.4a) and equiaxed grain zone (as shown at B zone in Fig.4a) alternately apart from the position near the bonding line.

Fig.5 illustrates the macrostructure of sample made by the divided-area forming and integral connection method. The macrostructures were distributed in the stripped method. Furthermore, most macrostructure stripes were parallel to the laser scanning direction (as shown at 1 and 3 positions in Fig. 5). While the macrostructure near the bonding line was different from those at other positions, and this phenomenon could be explained by the forming process. As shown at 2 and 4 positions in Fig.5, the macrostructure strips were not continuous. During the integral connection process, laser scanned the zone near the bonding line, built by divided-area forming. It led to re-melting of divided-area forming zone near the bonding line. The laser scanning routing paused a little time on the bonding line to guarantee the good bonding at the interface, which made the re-melting zone become larger than the formal size of molten pool when laser moved with consistent rate. After the remelting process the laser

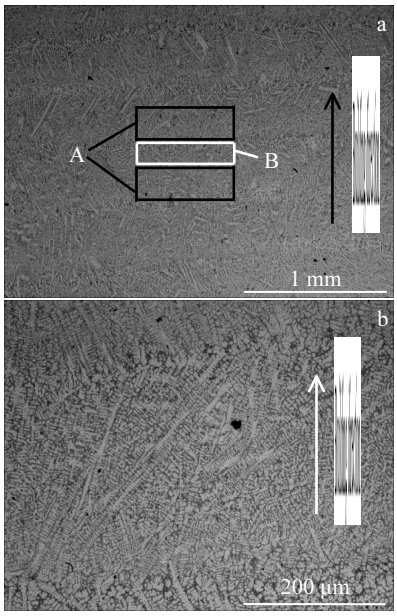

Fig.4 Microstructure of the XZ section of normal zone: (a) low magnification and (b) high magnification

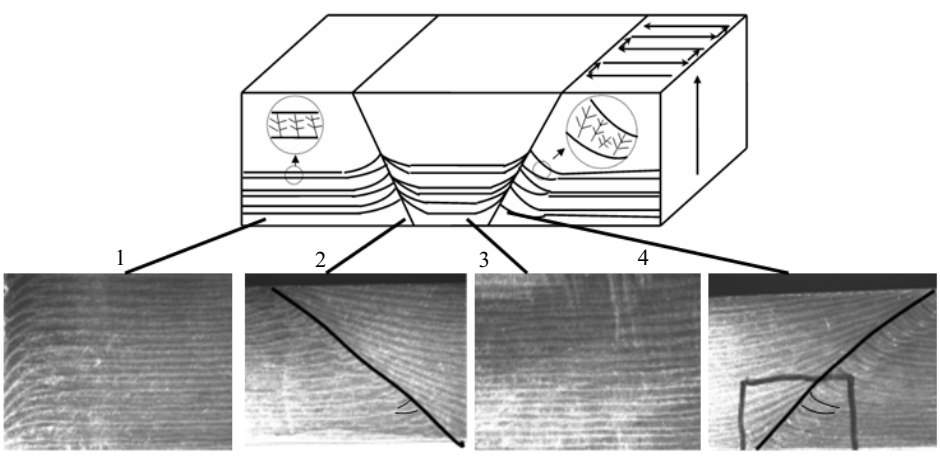

Fig.5 Macrostructures of XZ section at different positions

moved at a constant rate, which made the remelt zone become smaller. Finally the macrostructure stripe (the remelting line) flexed towards the building direction during the solidification process. The macrostructure strip in the integral connection zone was parallel to the laser scanning direction mostly, while the strip near the building line flexed towards building direction in continuous way, because the zone near the building line grew higher (along the building direction) than other positions.

The microstructure and grain size influence the mechanical properties of samples. The DAS (dendrite arm spacing) was often used to evaluate solidification microstructure[16]. Fig.6 shows an OM image near the bonding line. In comparison with the microstructures of the position apart from the bonding line as shown in Fig.4, microstructures in both of the two positions near the bonding line are different. The dendrite growth direction became multi-directional; at the same time the shorter average length of the primary dendrite arm and lager average SDAS (secondary dendrite arm spacing) were observed. The microstructures difference between positions near and apart from the bonding line is caused by the different laser scanning routes during the unique forming process. Totally, the microstructure of the samples build by the divided-area forming and integral connection method is distributed in dendrite, and the sizes of the microstructures (secondary dendrite arm spacing) are homogeneous.

2.2 Chemical composition distribution

The chemical composition distribution of the sample was discussed by scanning electron microscope and energy dispersive spectrometer (EDS). Five positions (1~5) spaced 13 cm apart along the scanning direction were selected to study the composition uniformity of the samples. The samples were built by the divided-area forming process with the size of 16 mm×70 mm×15 mm. The EDS results are listed in Fig.7. The positions 2 and 4 were in the bonding line zone. According to Fig.7, the composition was distributed homogeneously, and no significant macrosegregation appeared. The laser additive manufacturing processes underwent the building process of point-line-surface-object, the melting and solidification process happening in the moving molten pool influenced the composition distribution. The chemical homogeneity of metal powder feeding to molten pool, higher solidification rate and the limitation of flowing zone could guarantee homogeneous composition distribution.

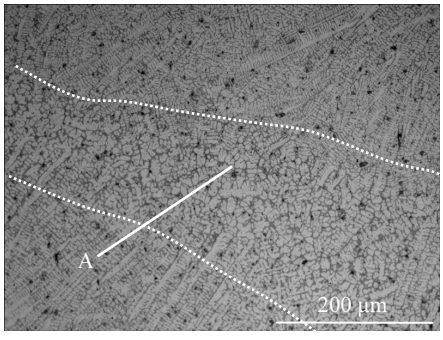

Fig.6 Microstructure of the XZ section near bonding line

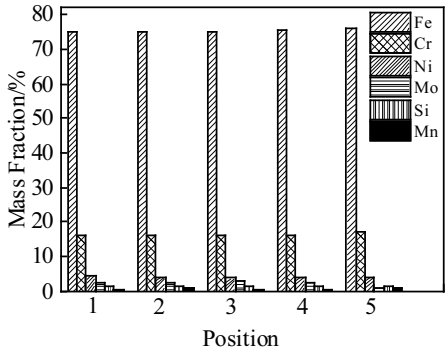

Fig.7 Chemical composition of XZ section at different positions 1~5

2.3 Phase composition

Fig.8a shows the microstructure of samples build by LENS, Fig.8b is the EDS line-scan analysis of the position A marked for test samples. According to the EDS was analysis result, element Cr was distributed more in the interdendritic zone than in the dendritic zone. This could be explained by the rapid solidification process. The moving molten pool underwent rapid solidification, and the microstructure grew by a dendritic method. The rapid solidification process could lead to dendritic segregation. Apart from basic metallic element and Cr, other elements were distributed homogeneously. The element composition influenced the phase composition, which

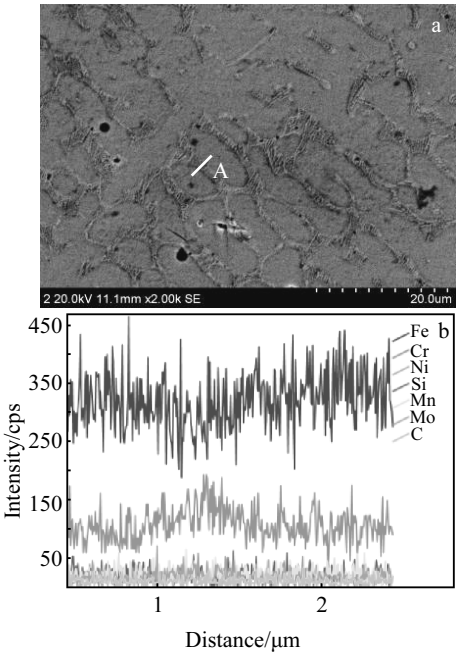

Fig.8 Microstructure (a) and EDS line scanning of the position A in Fig.8a (b)

were the key factors affecting the mechanical properties of the alloy. The influence of alloying element content on final phase composition have been discussed by many researchers. Schaeffler et al. used the equivalent equations to transfer the alloying element content to the Cr, Ni content. According to their researches, the composition phase of stainless steel by laser deposition could be determined by Schaeffler equivalent equation[17].

By the Schaeffler equivalent equation, formula (1) and (2)[17], the percentage of Cr_{eq} content was 18.44% and percentage of Ni_{eq} content was 8.5%. Compared with the Schaeffler diagram[18] in Fig.9 that the alloy was located in the A+F+M zone. Nevertheless, the element B influence and non-equilibrium solidification caused by high solidification rate were overlooked by the formula (1) and (2). This led to df ference of composition phase as the formula prediction. Ankur Gupta's research discussed the effect of B element on ferritic phase's stabilization in 17Cr-7Ni steel, and presented a new formula (3) [19]. According to formula (3), the addition of B leads to the equivalent Cr/Ni position moving to the A+F zone in the Schaeffler diagram. In order to make sure the composition phase of the alloy built by LENS, an XRD test was done. According to the XRD result as shown in Fig. 10, austenite and boride phase were found without the appearance of ferritic phase. Continuous and blocky-shaped second phase was distributed in the interdendritic zone. Based on the XRD result and the composition of the alloy, the second phase was $(FeCr)_xB$ boride.

$$Cr_{eq}=Cr+Mo+1.5Si+0.5Nb \quad (1)$$

$$Ni_{eq}=Ni+30C+0.5Mn \quad (2)$$

$$Cr_{eq}=Cr+1.5Mo+2Si+1.75Nb+5V+1.5Ti+5.5Al+0.75W+1.44B \quad (3)$$

$$Ni_{eq}=Ni+30C+0.5Mn+0.3Cu+Co+25N \quad (4)$$

Because Cr is the ferrite forming element in Fe-Cr-Ni alloy, the previous solidification process began with the appearance of γ austenite phase which had a lower content of Cr. Cr element segregation happened with the solidification processes executing. When the alloy liquid composition reached the

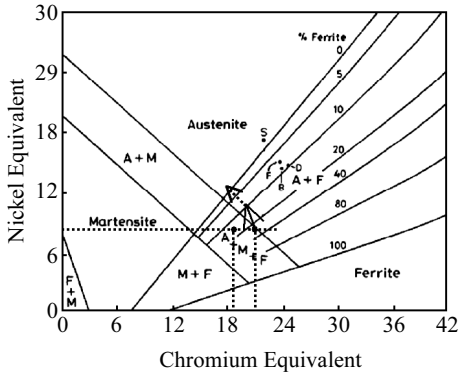

Fig.9 Schaeffler diagram showing the loci of each composition[17]

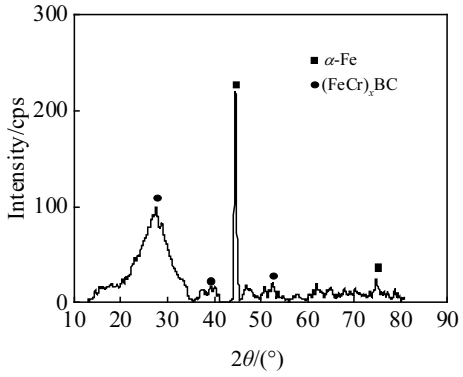

Fig.10 XRD pattern of tested samples

percentage range of boride and austenite eutectic precipitation, the non-equilibrium solidification happened with fast cooling rate. With the cooling processing, the austenite phase transformed into α phase. According to J. X. Fang research[20], the α phase is martensite.

Finally the interdendritic microstructures were $(FeCr)_xB$ and austenite eutectic phases. According to different position analyses, the microstructure phase composition of the whole sample was near, and no clear difference could be found.

2.4 Mechanical properties

The hardness of the alloy built by this method was tested. The alloy built by divided-area process had homogeneous hardness as shown in Table 2, which was bigger than 51 HRC. The micro-hardness was tested to study hardness changing near the bonding line, and results are listed in Fig. 11. According to the variation curve of micro-hardness, the bonding zone's hardness was near to other zones, which was caused by the homogeneous composition phase and microstructure.

The former built area near the left bonding zone (Fig. 11a) and right bonding zone near the right former build area (Fig. 11b) had lower hardness than other zones. The micro-hardness decreasing was mainly affected by microstructure difference. After the integral connection process, the edge of the former built section was re-melted by laser, and then solidified again. This made the microstructure discontinuous, and the growing direction of microstructure changed. The positions of the re-melting zone and the heat-affected zone near the bonding line might have lower hardness, but the difference was limited. The micro-hardness of continuous building zone was near.

Engineering stress-strain curve is presented in Fig. 12. All samples fractured without yield phenomenon, and the fractured positions were in the original gauge length. Ultimate tensile strength of the samples was a little bigger than 1300 MPa. Due to the fined structure and fined boride distributed in the interdendritic zone, the alloy had high strength caused by refinement strengthening and second-phase strengthening.

Table 2 HRC testing result of XZ section

Position No.	1	2	3	4	5
HRC	52.35	51.97	51.17	53.24	52.91

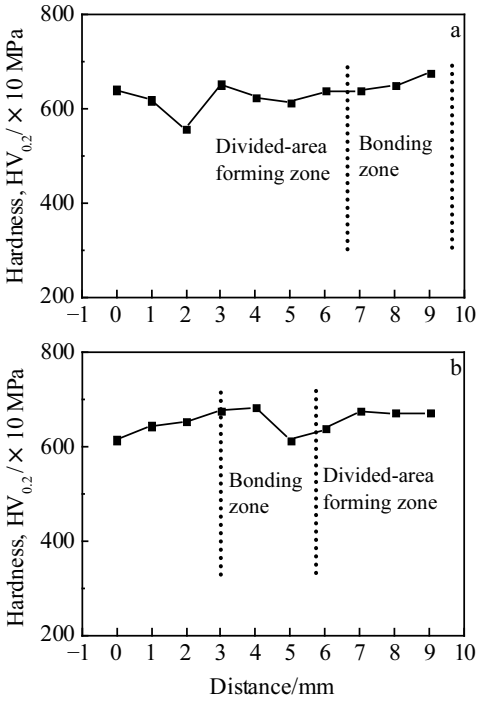

Fig.11 Microhardness of XZ section along scanning direction around left bonding line (a) and right bonding line (b)

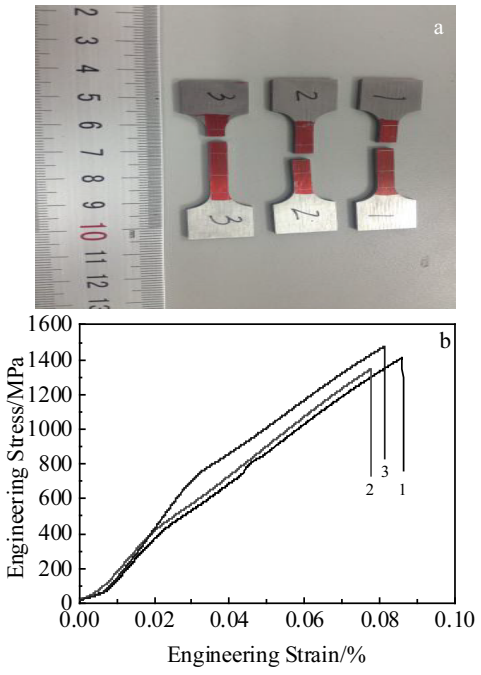

Fig.12 Tensile experiment result of samples: (a) fracture position of tensile specimen and (b) stress-strain curves

Nevertheless the boride distributed in mesh pattern decreased the alloy's deformability.

3 Conclusions

1) The microstructure of the Fe-Cr-Ni-B samples made by the divided-area forming and integral connection method consists of dendrites distributed in stripped method. The microstructure strips' directions between nearby areas of bonding line and other areas are different, and the microstructure strips flex towards building direction at nearby areas of bonding line.

2) According to the analysis of Schaeffler diagram, XRD, SEM and EDS, intermetallic phases consist of γ austenite phase, continuous/blocky-shaped boride and austenite eutectic phase distributed in the interdendritic zone.

3) Due to the fined structure and boride distributed in the interdendritic zone, the samples have high hardness (≥51 HRC), high ultimate strength and poor plastic deformability. The Vicker-microhardness near the bonding line is a little lower than that of other positions.

References

1 Huang Weidong, Lin Xin. *Materials China*[J], 2010, 29(6): 13 (in Chinese)

2 Tian Zongjun, Gu Dongdong, Shen Lida *et al. Aeronautical Manufacturing Technology*[J], 2015, 11: 38 (in Chinese)

3 Wang Huaming. *Acta Aeronautica et Stronautica Sinica*[J], 2014, 35(10): 2690 (in Chinese)

4 Chen Hongyu, Gu Dongdong, Gu Ronghai *et al. Chinese Journal of Lasers*[J], 2016, 43(2): 0 203 003

5 Li Meiyan, Han Bin, Gao Ning *et al. Chinese Journal of Lasers*[J], 2013, 40(5): 0 503 003

6 Liu Yang, Yang Yongqiang, Mai Shuzhen *et al*. *Materials and Design*[J], 2015, 87: 797

7 Song Menghua, Lin Xin, Liu Fenggang *et al. Materials and Design*[J], 2016,89:1035

8 Roberts Ibiye Aseibichin. *University of Wolverhampton*[J], 2012(1): 184

9 Ma Mingming, Wang Zemin, Wang Dengzhi *et al. Optics & Laser Technology*[J], 2013, 45: 209

10 Cabral Miramontes J A, Barceinas Sanchez J D O, Almeraya Calderon F *et al. Journal of Materials Engineering and Performance*[J], 2010, 19: 880

11 Li Kaibin, Li Dong, Liu Dongyu *et al. Applied Surface Science*[J], 2015, 340: 143

12 Sorour A A, Chromik R R, Gauvin R *et al. Materials Characterization*[J], 2013(1): 128

13 Krakhmalev P, Yadroitsava I, Fredriksson G *et al. Materials and Design*[J], 2015, 87: 380

14 Cheikh Hussam El, Courant Bruno, Branchu Samuel. *Optics and Lasers in Engineering*[J], 2012, 50: 1779

15 Khalid Rafi H, Starr Thomas L, Stucker Brent E. *Int J Adv Manuf Technol*[J], 2013, 69: 1299

16 Yin H, Felicelli S D. *Acta Materialia*[J], 2010, 58(4): 1455
17 Lo K H, Shek C H, Lai J K L. *Materials Science and Engineering R*[J], 2009, 65: 39
18 Milton Sergio Fernandes de Lima, Simon Sankaré. *Materials and Design*[J], 2014, 55: 526
19 Gupta Ankur, Bhargava A K, TewarI R *et al. Metallurgical and Materials Transactions A*[J], 2013, 43: 4248
20 Fang J X, Dong S Y, Wang Y J *et al. Journal of Manufacturing Processes*[J], 2017, 25: 402

基于分区成形激光增材制造一种 Fe-Cr-Ni-B 钢组织性能研究

赵宇辉，王志国，赵吉宾，施 凡
(中国科学院沈阳自动化研究所 装备制造技术研究室，辽宁 沈阳 110016)

摘 要：采用分区成形+整体连接的方式可以有效改善增材制造零件边缘处应力。本工作选用一种含 B 合金钢作为研究对象，对分区成形该合金组织形成机理、成分变化及性能变化进行了研究，验证分区成形该合金的组织、性能相容性。结果表明，该成形方式制备的合金组织由条带分布的树枝晶组成，靠近搭接线位置处组织条带出现向生长方向弯曲，整体上而言分区成形不同位置处组织尺寸差异性较小，合金无宏观偏析。合金中组成相由基体相奥氏体相、分布于枝晶间的硼化物+基体相共晶相构成，共晶相形成导致枝晶偏析。性能分析表明，由于硼化物的存在和组织细小，导致合金硬度高、强度高、塑性差，在熔接区域附近显微硬度略低于其他区域，但差异性不大，整体硬度分布较为均匀。

关键词：增材制造；分区成形；组织；性能；钢

作者简介：赵宇辉，男，1983 年生，硕士，副研究员，中国科学院沈阳自动化研究所，辽宁 沈阳 110016，电话：024-83601252，E-mail: yhzhao@sia.cn